

## MASS TRANSFER IN BINARY STARS USING SPH. II. ECCENTRIC BINARIES

CHARLES-PHILIPPE LAJOIE & ALISON SILLS  
Department of Physics and Astronomy, McMaster University,  
Hamilton, ON L8S 4M1, Canada  
*Draft version October 23, 2018*

### ABSTRACT

Despite numerous efforts to better understand binary star evolution, some aspects of it remain poorly constrained. In particular, the evolution of eccentric binaries has remained elusive mainly because the Roche lobe formalism derived for circular binaries does not apply. Here, we report the results of our Smoothed Particle Hydrodynamics simulations of mass transfer in eccentric binaries using an alternate method in which we model only the outermost layers of the stars with appropriate boundary conditions. Using this technique, along with properly relaxed model stars, we characterize the mass transfer episodes of binaries with various orbital parameters. In particular, we show that these episodes can be described by Gaussians with a FWHM of  $\sim 0.12 P_{\text{orb}}$  and that the peak rates occur after periastron, at an orbital phase of  $\sim 0.58$ , independently of the eccentricity and mass of the stars. The accreted material is observed to form a rather sparse envelope around either or both stars. Although the fate of this envelope is not modeled in our simulations, we show that a constant fraction ( $\sim 5\%$ ) of the material transferred is ejected from the systems. We discuss this result in terms of the non-conservative mass transfer scenario. We suggest our results could be incorporated in analytical and binary population synthesis studies to help better understand the evolution of eccentric binaries and the formation of exotic stellar populations.

*Subject headings:* binaries: close — stars: evolution — hydrodynamics — methods: numerical

### 1. INTRODUCTION

The study of exotic stellar populations (e.g. blue stragglers, low-mass X-ray binaries, helium white dwarfs) requires the understanding of close binary evolution. In turn, the study of binary evolution involves the use of many physical mechanisms occurring over dynamical, thermal, and nuclear timescales, which quickly render the problem at hand complicated. The analytical tools generally used to study binary stars have difficulty resolving all of these timescales; instead, they usually incorporate only some of the mechanisms or rely on analytical approximations. On the one hand, stellar evolution codes can evolve single stars over many billion years while taking into account convective mixing and different nuclear reactions networks. Only recently have they been used to evolve binary stars, although most of them are still in one dimension and only a handful use two dimensions (Han, Tout, & Eggleton 2000; Deupree & Karakas 2005). These binary evolution codes, along with population synthesis codes, which evolve many millions of stars at once over nuclear timescales (Portegies Zwart & Verbunt 1996; Hurley et al. 2002; Ivanova et al. 2005), rely on analytical prescriptions for the mass transfer and accretion rates. None of these techniques actually models the mass transfer itself as it often occurs on timescales that are too short. On the other hand, hydrodynamics is well suited for purposes such as mass transfer. However, it can be difficult to incorporate physical ingredients such as convective mixing, magnetic fields, radiative transfer or nuclear reactions. Hydrodynamics is also usually not designed to evolve stars over long periods of time. These difficulties therefore render the modeling of the long-term

hydrodynamical evolution of interacting binaries rather challenging.

The ideal case of circular orbits and conservative mass transfer has been studied intensively over the years. Seminal work by Morton (1960), Paczyński (1965, 1971) and Paczyński & Sienkiewicz (1972), among others, on mass transfer and its consequences on the stars and the orbital parameters have opened the way to a more quantitative study of binary evolution. Iben (1991) and Iben & Livio (1993) have more recently laid out the overall evolutionary paths of many different binary populations and explained the formation scenarios of many exotic objects. But, from a theoretical point of view, a detailed description of some aspects of close interactions are still lacking. Of particular interest are the rate at which mass is transferred from one star to the other, the amount of mass accreted by the secondary stars, and the degree of mass loss from these systems, if any. To date, these quantities have usually been either approximated from theoretical estimates or arbitrarily fixed. But because these quantities are critical for understanding the long-term evolution of binary stars, as they are some of the mechanisms that drive the change of orbital separation and ultimately dictate the fate of binaries, it is important to get better estimates for the more realistic, non-idealized cases. In particular, recent studies (Sepinsky et al. 2007a, 2007b, 2009) have suggested that eccentric binaries may evolve differently when compared to circular binaries. Given that a non-negligible fraction ( $\sim 20\%$ ) of interacting binaries have eccentric orbits (Petrova & Orlov 1999; Raguzova & Popov 2005), this could arguably modify the formation rates and total numbers of binary and exotic populations in synthesis models. Therefore, a better understanding and calibration of the mass transfer rates, the degree of mass

loss from binary systems, and the accretion process are needed in order to get a better, more realistic picture of the exotic stellar populations.

In this paper, we present the results of hydrodynamical simulations of mass transfer in eccentric binaries using a specifically designed SPH code (Lajoie & Sills 2010; hereafter Paper I). We model two different binary systems with various eccentricities and semi-major axes and concentrate on how and when mass transfer is initiated, as well as how much mass is accreted by the companion star and/or lost from the system.

## 2. BRIEF THEORY OF ECCENTRIC BINARY SYSTEMS

Although most short-period binaries are on circular orbits, many relatively close binaries also have eccentric orbits in which mass transfer can occur only close to periastron. Such episodes of mass transfer are usually not taken into account in binary population synthesis studies since rapid circularization at the onset of mass transfer is often assumed. To some extent, such episodes of mass transfer could modify the general picture of exotic star populations, especially in dense clusters where the formation of eccentric binaries through captures is more likely. However, most of the theoretical background generally used applies only to circular orbits, and one must rely on other approximations to estimate the rate of mass transfer in eccentric binaries, as we now discuss.

### 2.1. Roche lobe and equipotentials

Using analytics to investigate the equations of motion in binary systems, Sepinsky et al. (2007a) showed that eccentric binaries undergoing mass transfer can behave quite differently when compared with circular binaries. Indeed, the authors found that the Roche lobe radius (denoted  $R_L$ ) can be smaller than the circular case by more than 20% for binaries with mass ratios close to unity and rotating faster than the orbital velocity at periastron. The reverse is also true, as binaries rotating slower than the orbital velocity at periastron can have a Roche lobe radius  $\sim 10\%$  larger than the circular case. Moreover, depending on the degree of asynchronicity and eccentricity, the geometry of the equipotential surfaces is found to change significantly and allow for some mass to be ejected from the system through the  $L_1$  point. Sepinsky et al. (2007a) found that the usual Roche lobe can sometimes open up around the secondary star, allowing for some mass loss through the  $L_1$  point, and that the potential at the  $L_3$  point can sometimes be only slightly larger than that at the  $L_1$  point, also allowing for some more mass loss (see Figure 7 of Sepinsky et al. 2007a). Although we expect some mass to be ejected from the system, the total amount lost is hard to estimate and authors have generally used some parameterizations to study the effect of non-conservative mass transfer on the evolution of binaries (Sepinsky et al. 2009; hereafter, SWKR09). These results suggest that eccentric and asynchronous binaries are likely to undergo mass transfer at earlier phases of their life (compared to circular binaries) and that the latter is most likely non-conservative. Note that Dermine et al. (2009) finds similar changes to the shape of equipotentials when considering the effect of radiation pressure in *circular* and *synchronized* binaries.

These recent works emphasize that the classical Roche model is not adequate in most instances. The addition of realistic physical ingredients (e.g. asynchronism, eccentricity, radiation pressure) in the models of binary stars modifies the structure of equipotentials. The Roche lobe model derived for circular orbits therefore does not apply.

### 2.2. Secular evolution

Based on their previous results, Sepinsky et al. (2007b) (hereafter, SWKR07) and SWKR09 went on to study the secular evolution of eccentric binaries undergoing mass transfer, with the assumptions of instantaneous mass transfer ( $\dot{M}_0 = 10^{-9} M_\odot/\text{yr}$ ) centered at periastron and both conservative and non-conservative mass transfer. The authors found that depending on the mass ratio and eccentricity, the secular changes of orbital separation and eccentricity can be positive or negative, and can occur on timescales ranging from a few million years to a few billion years. Moreover, these timescales can, in some cases, be comparable to the orbital evolution timescales due to tidal dissipation, which can be additive or competitive. Based on these findings, the authors suggest that the usual rapid circularization assumption is not always applicable and, in some cases, very unlikely. Finally, SWKR09 conclude that relaxing the assumption of conservative mass transfer does not change the overall conclusions of their previous work (SWKR07). The rates of secular evolution for  $a$  and  $e$  found by SWKR07 and SWKR09 are directly proportional to the assumed mass transfer rate. However, this can be hard to constrain with analytical prescriptions only. Indeed, when mass transfer occurs periodically, binaries can remain on eccentric orbits for long periods of time, making the Roche lobe radius and the mass transfer rate difficult to determine, as the latter depends on the degree of overflow ( $\Delta R = R_* - R_L$ , where  $R_*$  is the radius of the star).

### 2.3. Previous simulations of mass transfer

One way to better estimate the rates of mass transfer is by using hydrodynamical simulations. Only a handful of such simulations have been done to this day. Despite usually not being suited for long, thermal- or nuclear-timescale studies, hydrodynamical simulations can be useful for understanding transient phenomena and episodes of dynamical mass transfer.

Only a few authors have investigated the hydrodynamics of eccentric binaries. Regös et al. (2005) (see also Layton et al. 1998) studied the shape of the equipotential surfaces in eccentric binaries using both analytical and numerical (SPH) approaches. Their findings agree with those of Sepinsky et al. (2007a) in that mass transferred through the  $L_1$  point close to periastron passages may leave the system (as well as through the  $L_2$  point). However, their estimates for the Roche radius are larger and similar to the Roche lobe radii for the circular and synchronized case. Interestingly, the authors also study the onset of mass transfer along the orbit for one binary and different eccentricities. The low resolution of these simulations (10,000 particles), however, does not allow for accurate mass transfer rate determinations.

Church et al. (2009) have partially circumvented this problem using an innovative SPH technique for modeling mass transfer in cataclysmic variables, where the least

massive star is losing mass to a compact white dwarf. With the aim of getting better estimates of mass transfer rates, their innovative approach allows for high *mass* resolution in the outer parts of the star and therefore for the resolution of low mass transfer rates. Despite using a relatively low number of particles ( $\sim 40,000$ ), most of the stars' mass is contained in a few very massive particles, allowing for the outer particles to have relatively low masses. By varying the eccentricity and periastron distances for one particular mass ratio ( $q_2 = 0.6$ ), the mass transfer rates they obtain show qualitative behaviour in agreement with the photospheric mass transfer rate predicted by Ritter (1988). Edwards & Pringle (1987) performed grid-based hydrodynamics calculations of polytropic semi-detached systems and compared the mass transfer rates to analytical estimates, with which they find good agreement. However, their simulations only modeled a small rectangular box close to the  $L_1$  point and did not encompass either the donor or the accretor and did not assess whether mass was lost from the system.

Finally, in some simulations to date, the accreting star is not realistically modeled but rather often modeled as a point mass or with surface boundary conditions. These simplifications prevent from drawing any quantitative conclusions regarding the accretion process. Moreover, as pointed out by Sills & Lombardi (1997), the use of polytropes instead of realistic models may lead to significantly different internal structures for collision products, which may arguably be applicable to interacting binaries. Therefore, more work remains to be done in order to better understand how mass transfer operates and affects the evolution of eccentric binary systems.

### 3. COMPUTATIONAL METHOD

For a more realistic modeling of hydrodynamical mass transfer, it is better to use hydrodynamics techniques since they can easily be adapted to model binary systems in three dimensions and physically follow the transfer of mass from one star to the other. Here, we use an SPH code based on the version of Benz (1990) and Bate et al. (1995) with a recent updated treatment of boundary conditions specifically designed to model boundary stars presented in Paper I. We model our stars from theoretical profiles obtained from our stellar evolution code (YREC; Guenther et al. 1992) and distribute SPH particles on an hexagonal lattice while iteratively assigning particle masses so that the density profile matches that from our stellar evolution code. Binaries are relaxed in their own gravitational force (and centrifugal force) prior to the start of the mass transfer simulations (see Paper I). Using our treatment of boundary conditions, we replace the inner particles with a central point mass and model only the outermost layers of the stars. The location of the boundary is, at this point, arbitrary but should be placed at least a few smoothing lengths from the surface. Use of our boundary conditions allows for better spatial and mass resolutions in the mass transfer stream as well as the use of less CPU time. Note that each particle's smoothing length is also consistently evolved in time, following the prescription of Benz (1990), allowing for a better spatial resolution in regions of high density. Finally, we use Monaghan's viscosity (Monaghan 1989) with  $\alpha = 1.0$  and  $\beta = 2.0$  along with an adiabatic equa-

tion of state of the form  $P = (\gamma - 1)\rho u$ , where  $\gamma = 5/3$ ,  $\rho$  is the density and  $u$  the internal energy (per unit mass).

### 4. MASS TRANSFER IN ECCENTRIC BINARIES

We now present the results of our simulations of mass transfer for two different binary systems and discuss the overall behaviours observed in our simulations. In particular, we are interested in the mass transfer rates and properties involved in such close interactions. We have modeled binary systems with stars of different masses, semi-major axes, and eccentricity. The different orbital parameters modeled for both system are summarized in Table 1 along with some preliminary results.

#### 4.1. $0.80 M_\odot + 0.48 M_\odot$

Our first model consists of a low-mass binary system representative of the turn-off mass of globular clusters. The initial separation of this binary system, at apastron, is set to  $4 R_\odot$  such that the stars do not initially overflow their Roche lobe. The boundary is set at  $0.8 R_\odot$  for the  $0.8\text{-}M_\odot$  star and  $0.35 R_\odot$  for the  $0.48\text{-}M_\odot$  star, both corresponding to  $\sim 75\%$  of the stars' radii. At this radius, most of the mass of the stars is encompassed within the central point mass. The total number of particles is  $\sim 600,000$  and the total mass of SPH particles is  $\sim 4 \times 10^{-3} M_\odot$  and  $\sim 3 \times 10^{-2} M_\odot$  for the  $0.8\text{-}$  and  $0.48\text{-}M_\odot$  stars respectively. Using SPLASH (Price 2007), a publicly available visualization tool for SPH simulations, we show in Figure 1 the logarithm of the density, in the  $XY$  plane, for the case with  $e = 0.25$ . The time is shown in units of the dynamical time ( $\tau_{dyn} = \sqrt{R_\odot^3/GM_\odot} \simeq 0.5$  hour) and the orbital period corresponds to  $\sim 32 \tau_{dyn}$ . Each image is  $12 R_\odot$  by  $12 R_\odot$ , and the density scale ranges from  $10^{-10} \text{ g cm}^{-3}$  (dark) to  $1 \text{ g cm}^{-3}$  (white). The  $0.8\text{-}M_\odot$  star is the larger of the two stars and the large density contrast between the two stars is obvious from these plots. Mass transfer occurs only periodically, close to periastron, and shuts off when the stars are further apart. Moreover, the secondary is retaining some of the transferred mass, forming an envelope, whereas the primary does not seem to be affected strongly from losing mass. The density of the accreted material around the secondary is much lower than that of the secondary's surface layer and this may have some implications for the long-term accretion of this material (see § 4.4). Some mass is also lost from the secondary's far side through the  $L_2$  point whereas no mass is lost through the primary's far side through the  $L_3$  point. The whole system eventually becomes engulfed in a relatively warm but low-density envelope that extends for many solar radii. Finally, the mass transfer proceeds relatively smoothly and no shocks are observed at the surface of the secondary. Moreover, it is observed that the mass transfer stream in between the two stars is relatively cooler than the surrounding envelope, since its expansion comes at the expense of its own internal energy.

Figure 2 shows the different energies, normalized to their initial value, as a function of time for the same system. The total energy is fairly well conserved during the whole duration of the simulation. It varies by at most  $\sim 3\%$  and seems to do so periodically. The eccentricity of this system is obvious from the shape of the curve of the kinetic energy as it peaks at periastron,

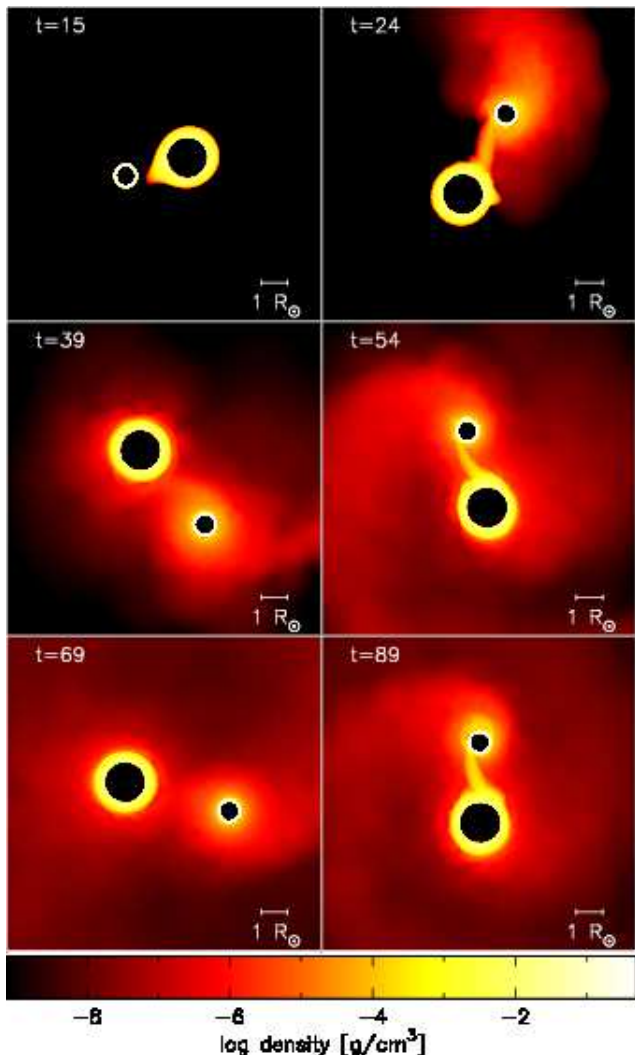


FIG. 1.— Logarithm of the density in the  $XY$ -plane for the  $0.80 + 0.48 M_{\odot}$  binary and  $e = 0.25$ . Each image is  $12 R_{\odot}$  by  $12 R_{\odot}$  and the central point masses are not shown. The time is shown in units of the dynamical timescale ( $\tau_{dyn}$ ) and the orbital period is  $\sim 32 \tau_{dyn}$ .

halfway through the orbital period, and decreases almost to its initial value. The different values of the extrema of the kinetic energy suggest that the orbital separation is changing. Similar behaviours are also observed for models with different eccentricities. As for the gravitational energy, it varies in the same way as the kinetic energy, whereas the thermal energy stays constant to within less than 0.5% over the whole duration of the simulation. The total angular momentum, on the other hand, varies around its initial value, by no more than 2.5% over the whole duration of the simulation. We use the binary’s centre of mass as the rotation axis to calculate the total angular momentum of the system and all of the angular momentum is, as expected, in the  $z$ -direction, i.e. perpendicular to the orbital plane. The angular momentum in the other directions is at least 4 orders of magnitude smaller and remains negligible for the whole duration of the simulations. These variations of the total angular momentum observed in our simulations are acceptable given that the angular velocity of the ghosts is artificially

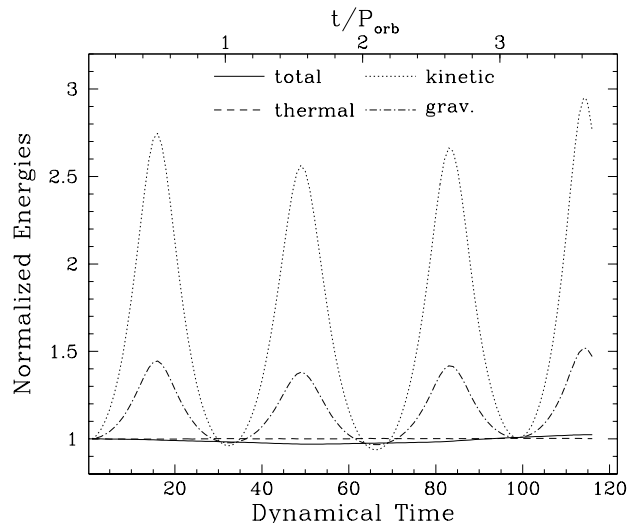


FIG. 2.— Different energies as a function of time for the  $0.80 + 0.48 M_{\odot}$  binary with  $e = 0.25$ .

maintained at a fixed value (see Paper I).

#### 4.2. $1.50 M_{\odot} + 1.40 M_{\odot}$

The second system we model is a higher-mass binary representative of the population of relatively old open clusters. Also, since the secondary is much larger and its density is of the same magnitude as the primary, we expect the infalling material to interact much more dynamically with the envelope of the secondary. The two stars are initially set at a separation of  $6 R_{\odot}$ , at apastron, which places them well within their Roche lobe. The location of the boundaries is chosen at 75% of the total radius of the stars, corresponding to a radius of  $1.05$  and  $0.90 R_{\odot}$  for the primary and the secondary respectively. The total number of particles is  $\sim 440,000$  and, consequently, the total mass in SPH particles in the primary amounts to  $\sim 1.16 \times 10^{-3} M_{\odot}$  whereas the secondary contains  $\sim 1.65 \times 10^{-3} M_{\odot}$  of SPH particles. The remainder of the mass is contained in the central point masses. Figure 3 shows the logarithm of the density in the  $XY$  plane for the  $e = 0.25$  case at different times. The orbital period for this system is  $\sim 39 \tau_{dyn}$ . The interaction between the two stars is much stronger here, as material from both stars is lost, and a clear spiral pattern is observed and most prominent towards the end of each mass transfer episode (i.e. after each periastron passage). At low eccentricity, the mass transfer is rather smooth and has little effect on the secondary, whereas for our largest eccentricity runs, the systems almost come into contact at periastron and material from the primary plows through the secondary’s envelope, which is pushed around the whole system. Most of the envelope surrounding both stars is relatively hot as it gets heated up after the first periastron passage. Also, unlike the low-mass binary, we observe mass loss through both the  $L_2$  and  $L_3$  points, which may be enhanced by the fact that asynchronism is substantial at periastron, thus lowering the potential at the  $L_3$  point (see §2.1).

We show the different energies and total angular momentum for the same simulation in Figures 4. The different energies oscillate as a function of the orbital position, with the kinetic and gravitational energies reaching ex-

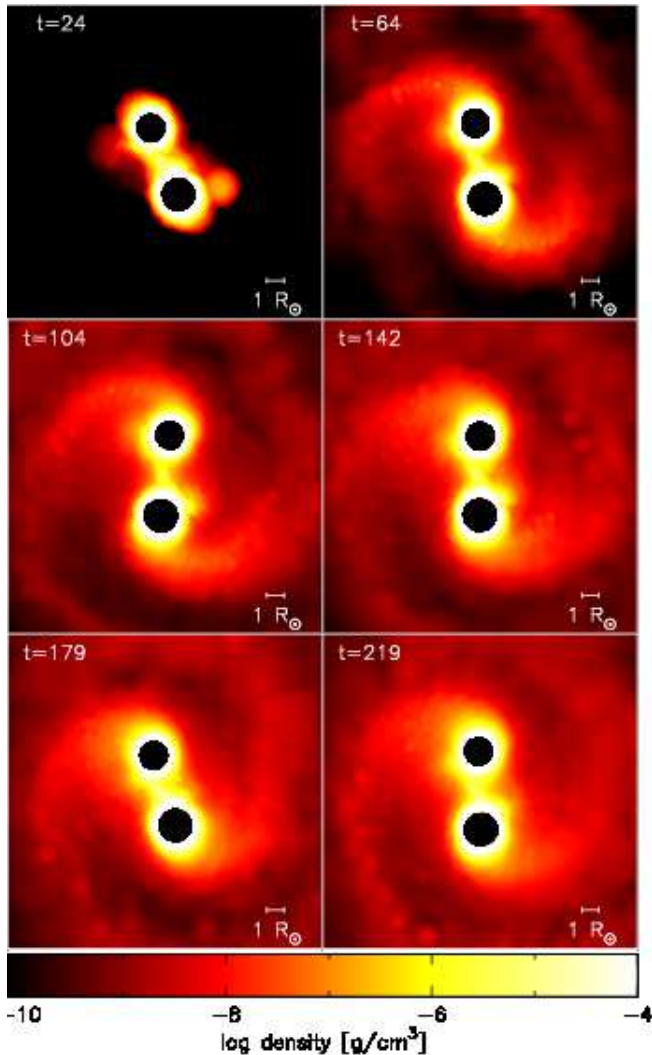


FIG. 3.— Logarithm of the density in the  $XY$ -plane for the  $1.50 + 1.40 M_{\odot}$  binary and  $e = 0.25$ . Each image is  $18 R_{\odot}$  by  $18 R_{\odot}$  and the central point masses are not shown. The time is shown in units of the dynamical timescale ( $\tau_{dyn}$ ) and the orbital period is  $\sim 39 \tau_{dyn}$ .

trrema at periastron. The kinetic energy always peaks at the same value and comes back to its initial value when at apastron, suggesting that the binary is well relaxed and that it follows the orbit it was initially put on. Also, the total energy changes by no more than  $\sim 0.5\%$  over the whole duration of the simulation. We also notice that the total internal energy slowly increases, by 8% at the end of the simulation. This change in thermal energy comes at the expense of gravitational energy, but although 8% seems substantial, we emphasize that the total thermal energy represents roughly only 1 part in 1000 of both the kinetic and gravitational energies. Therefore, it would be hard to observe such a small change in gravitational energy on the scale of Figure 4. The total angular momentum of the system and of the two stellar components also remains constant during the entire simulation to a 1% level for the whole duration of the simulation.

#### 4.3. Mass transfer rates

We now determine the mass transfer rates from our simulations. We use the method based on the total en-

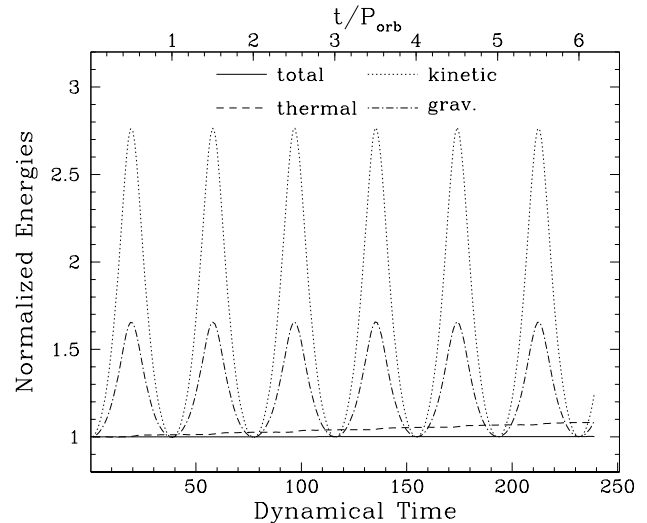


FIG. 4.— Different energies as a function of time for the  $1.50 + 1.40 M_{\odot}$  binary with  $e = 0.25$ .

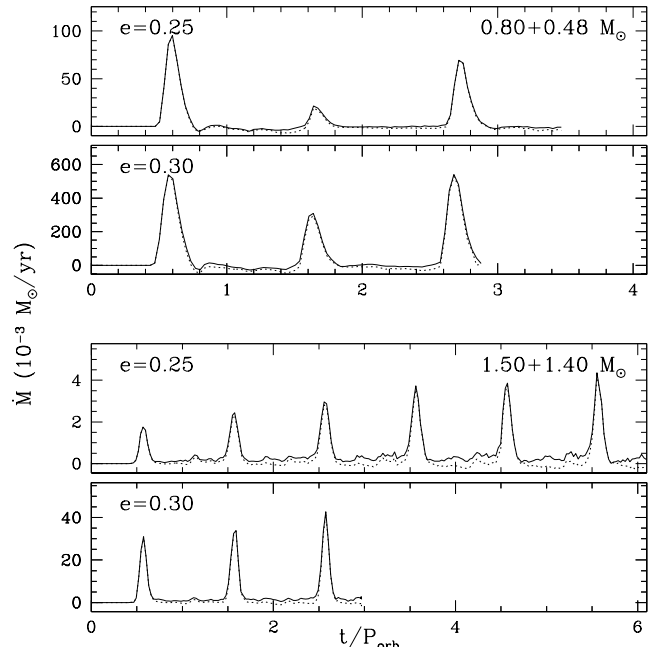


FIG. 5.— Mass transfer rates as a function of orbital period and eccentricity for a selection of runs from the  $0.80 + 0.48 M_{\odot}$  (upper two panels) and the  $1.50 + 1.40 M_{\odot}$  (lower two panels) binaries. The solid and dotted lines represent the mass transfer and accretion rates of the primary and secondary respectively.

ergy of each SPH particle, as discussed in Paper I (see also Lombardi et al. (2006)), to determine to which component SPH particles are bound. Particles are assigned to one of the following components: the primary and secondary stars, the binary envelope, and the ejecta.

##### 4.3.1. Rate and duration of mass transfer

Figure 5 shows some of the mass transfer and accretion episodes a function of time and eccentricity for the stellar components in the  $0.80 + 0.48 M_{\odot}$  and  $1.50 + 1.40 M_{\odot}$  systems. For the primary (solid lines), we plot the negative of the mass transfer rates so that we can compare it to the (positive) accretion rate of the secondary.

In most cases, the mass transfer rates are well defined and peak right after the periastron passages. We note that mostly particles from the outer envelope of the primary only are transferred during each episode and that the boundary never becomes involved in the interaction. For the low-mass binary, mass transfer occurs only for eccentricity greater than  $\sim 0.20$ . In these cases, the mass transferred from the primary is almost totally accreted by the secondary, as shown by the reciprocity of the solid and dotted lines. We note also that both rates sometime dip in the negative part of the plots, meaning that some material is falling back onto the primary or that the secondary is losing some of its newly-accreted mass. For lower eccentricities (e.g.  $e = 0.10 - 0.20$ ), only a few particles are actually transferred and either the mass transfer is insignificant or the code fails to correctly handle the few tens of particles wandering in between the two stars. Finally, we note that there is no trend in the maximum mass transfer rates of the low-mass binary, although the need for a larger number of orbits might be required to observe any such trends. The changes in the maximum mass transfer rates observed are likely due to the fact that the stars do not remain on their initial eccentric orbit, as can also be seen in Figure 2, therefore changing the degree of overflow and the mass transfer rate.

The high-mass binary simulations, on the other hand, all display the characteristic episodic mass transfer peaks, with increasingly larger mass transfer rates. Interestingly, the maximum mass transfer rates once again all peak shortly after periastron, although the two smallest eccentricities show quite a bit of noise in between these peaks. The noise is caused by material falling back onto either or both stellar components in between periastron passages. In most instances, the material lost by the primary is almost all accreted onto the secondary, although the accretion rates of the secondary shows some differences with respect to the mass loss rates of the primary, suggesting that some mass is lost from the system. The  $e = 0.20$  case is rather noisy and there seems to be a significant fraction of the mass transferred that falls back onto the primary and secondary after the main episodes of mass transfer. This seems to be important only in the smaller eccentricity cases. The primary's mass transfer rates rarely becomes negative, unlike the secondary's accretion rates, which are mostly negative in between periastron passages, suggesting that the secondary loses mass. We note however that mass becomes bound to the secondary (and the primary) only temporarily as subsequent episodes of mass transfer are sometimes energetic enough to plow through the surrounding envelope of the secondary and eject some of this material. Likewise, the maximum mass transfer rates are observed to increase both with time and eccentricity. Given that both stars remain very close to their initial eccentric orbit (see Figure 4), this increase in the peak mass transfer rate is likely due to an increase of the primary star radius. Figure 6 shows the radii enclosing different fractions of the total bound mass for the primary. The periastron passages are clearly visible and, most importantly, the radii *in between* the mass transfer episode gradually increase, which is indicative of the expansion of the primary's envelope as matter is being lost. This increase in radius inevitably leads to an increase in the degree of overflow and, consequently, the mass transfer rate. We also note

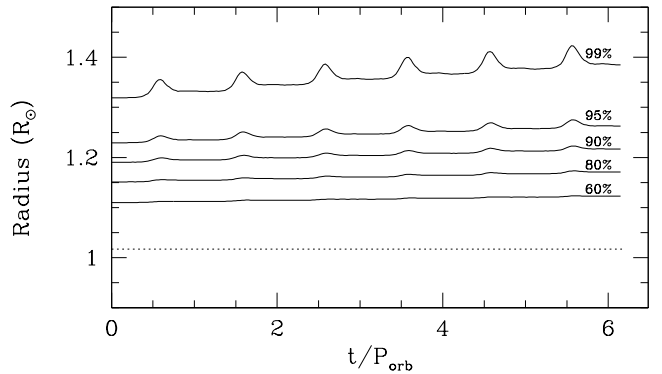


FIG. 6.— Radii enclosing different fractions of the total bound mass (in SPH particles) to the primary star as a function of time for the  $1.40 + 1.50 M_{\odot}$  binary with  $e = 0.25$ . The dotted line represents the location of the boundary.

that the boundary is well within the star and the radius containing 60% of the mass in SPH particles barely changes with time, indicative that tidal effects are negligible at this location. Finally, we note the similarities between the two systems modeled in the position, duration, and shape of the mass transfer rate episodes. In particular, their shape is suggestive of a Gaussian function.

The range of mass transfer rates observed in our simulations ranges from a few  $10^{-6} M_{\odot} \text{ yr}^{-1}$ , for the high-mass binary with  $e = 0.15$ , to  $0.1 M_{\odot} \text{ yr}^{-1}$  for the low-mass binaries. We emphasize that these relatively high mass transfer rates last only for a short period of time (i.e.  $\sim 0.20$  orbit) and the total mass transferred amounts to less than  $\sim 10^{-4} - 10^{-5} M_{\odot} \text{ yr}^{-1}$  per periastron passage. In all cases, the number of particles transferred ranges from a few hundreds to many thousands per mass transfer episode. Binaries where the number of particles transferred is less than  $\sim 100$  are considered as not transferring mass on the basis of the poor SPH treatment for such low numbers (see Table 1). Given the least massive particles in our simulations, the lowest possible mass transfer we can model (notwithstanding the numerical noise), is of the order of  $10^{-7} - 10^{-6} M_{\odot} \text{ yr}^{-1}$ , which is comparable to that of D'Souza et al. (2006). However, given the low number of particles that would be transferred in such instances, the SPH approach fails at properly evaluating the hydrodynamical forces on these isolated particles. We compare our results with theoretical expectations in §5.

#### 4.3.2. Gaussian fits to mass transfer episodes

Using our mass transfer rate profiles of Figure 5, we now fit a Gaussian function to every mass transfer episode. The general Gaussian we use has the following form:

$$\dot{M}(t) = A \exp\left(-\frac{(t-\mu)^2}{2\sigma^2}\right) + D \quad (1)$$

where  $A$  is the maximum amplitude,  $\mu$  is the centre of the Gaussian,  $\sigma$  is proportional to the width of the Gaussian and  $D$  is the background (or continuum) mass transfer rate. The latter parameter is used to measure the background noise as in some case the mass transfer rates do not fall back to zero in between mass transfer episodes. All the free parameters are fitted using the

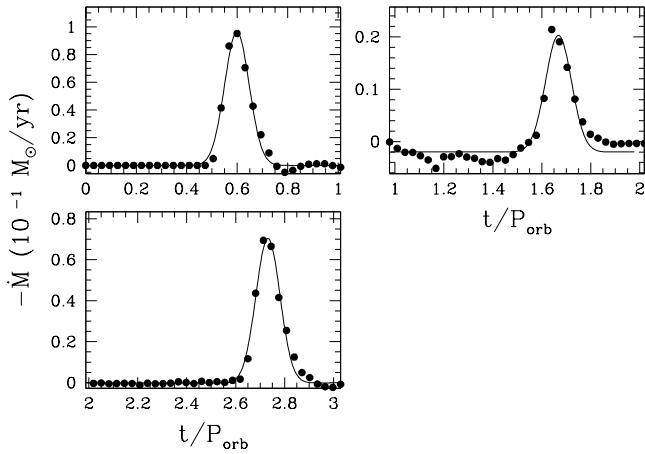


FIG. 7.— Gaussian fits to the primary’s mass transfer episodes for the  $0.80+0.48 M_{\odot}$  binary with  $e = 0.25$ . The values of the fitted parameters are reported in Table 2.

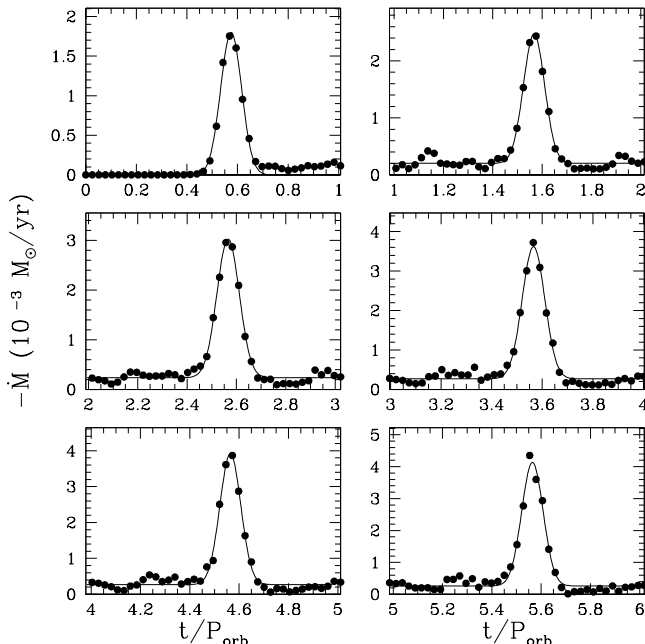


FIG. 8.— Gaussian fits to the primary’s mass transfer episodes for the  $1.50+1.40 M_{\odot}$  binary with  $e = 0.25$ . The values of the fitted parameters are reported in Table 2.

nonlinear least-squares method of Levenberg-Marquardt (Press et al. 1992). We fit the height of the Gaussian extended wings so that the width of the Gaussian matches more closely the data points. However, in cases where matter falls back onto the stars between periastron passages, the fitting procedure is to be taken with care. Examples of the Gaussian fits to the mass transfer episodes are shown in Figures 7 and 8 for two of our simulations. The parameters obtained from the fitting procedure are given in Table 2. Some data points are assigned a relatively large error since they are part of the pre-periastron mass transfer episodes and do not contribute to the main episode of mass transfer nor to the fitting procedure. Note that doing so does not significantly change the values of both  $\mu$  and  $\sigma$ . Moreover, for every first episode of mass transfer, we do not fit the continuum (parameter

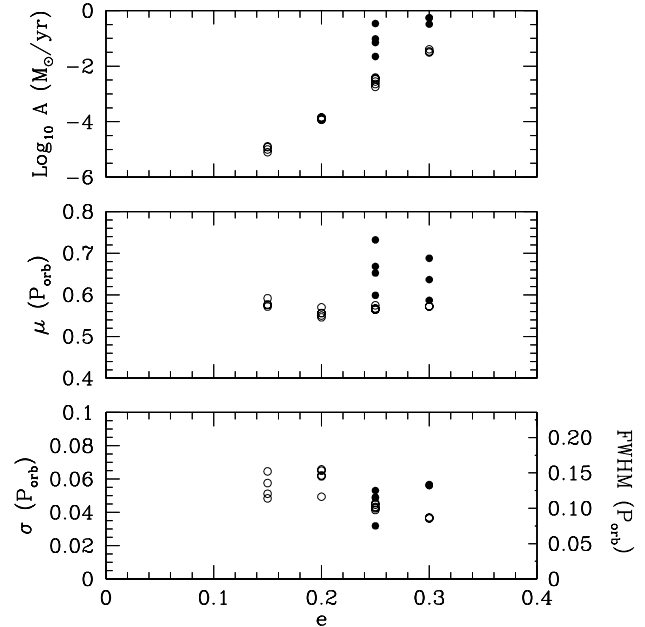


FIG. 9.— Amplitude, position, and width of the Gaussian fits to the mass transfer episode for the primary as a function of eccentricity for both binary systems. Solid dots are for the  $0.80 + 0.48 M_{\odot}$  binary while open dots are for the  $1.50 + 1.40 M_{\odot}$  binary. See also Table 2.

$D$ ) as we expect the value of the mass transfer rate prior to the first periastron passage to be identically zero. We do not fit this parameter for any subsequent peak however.

For most of our simulations, Gaussians fit the data points remarkably well. In most cases, the amplitude, centre, and width all closely match the data points. Again, for cases where matter is observed to fall back onto the stars, the fits to the height of the extended wings is obviously not as reliable. For example, the Gaussian fit for the low-mass binary with an eccentricity  $e = 0.20$  is not reliable as the mass transfer is too noisy. An important source of uncertainty on these fitted parameters, especially  $A$  and  $D$ , is the noise on either side of the peaks seen in the data. On the other hand, the width and amplitude of most (if not all) of the mass transfer episodes are well matched by Gaussians.

We plot, in Figure 9, the amplitude, centre, and width of all the Gaussians we fitted as a function of eccentricity. Many trends can be seen in this plot. First, the maximum mass transfer rate increases with the eccentricity. This is expected since as the eccentricity increases, the periastron distance gets smaller and the two stars get closer to each other, thus facilitating mass transfer. Our results also suggest that the maximum mass transfer rate increases linearly with the eccentricity, although we also expect a cut-off at low eccentricity where the primary will not fill its Roche lobe even when at periastron. Also, although we only have two data points from our low-mass binary simulations, these two simulations suggest a similar trend. As for the position where the maximum mass transfer rate occurs, the results from our high-mass binary simulations clearly show that mass transfer rates peak at an orbital phase slightly larger than periastron, around  $0.55 - 0.57$ . Although mass transfer starts around periastron, it only peaks later when the two stars have already started getting further away from

each other. This is in contrast with one of the basic assumptions of SWKR07 and SWKR09, who assumed that mass transfer occurred instantaneously at periastron. The observed delays in the peak mass transfer rates are consistent with a free-fall time ( $\tau_{ff} \simeq 0.5(G\bar{\rho})^{-1/2}$ ) into the secondaries' potential well at periastron. Following Eggleton (1983), the free fall times for our systems should be about  $0.05 - 0.065 P_{orb}$ , similar to the delays observed in our simulation (see e.g. Table 2), with an expected slight increase for the low-mass binaries. It seems likely therefore that the small differences in the position of the mass transfer rate peaks observed in our simulations are real. Our method for determining the mass transfer rates does not tell whether a particle *will* be transferred but rather if it has been transferred, which is what we define as mass transfer, and our results seem to indicate that this occurs over a free-fall time. Only at periastron is the tidal force large enough to strip the deeper layers of the primary. Since this material has to travel to the Roche surface before being assigned to the secondary, a delay in the peak mass transfer rate is to be expected. We note that such delays in the peak mass transfer rates should be intrinsic to eccentric binaries as these systems never exactly fill their Roche lobe but rather periodically shrink within and expand beyond it. Although the results from our low-mass binary simulations are less suggestive, the delays observed in the position of the maximum mass transfer rate also suggest that the maximum degree of overflow should occur later than periastron.

Finally, we also observe in both sets of simulations that the width (or duration) of the mass transfer episode is finite in time and arguably independent of the eccentricity. Our results suggest that the full width at half maximum ( $\text{FWHM} \approx \sqrt{8 \ln 2} \sigma$ ) is approximately  $0.10 - 0.13 P_{orb}$ . One could argue that there is a small negative slope suggesting that the higher the eccentricity, the faster the mass transfer occurs, which is plausible since stars on high eccentric orbits spend less time around periastron compared to star on low eccentric orbits. No matter the trend, this value of the width of the mass transfer rates is also in contrast with another basic assumption used by SWKR07 and SWKR09, who assumed an instantaneous mass transfer rate. Our results clearly show that this is not the case and that the mass transfer occurs over an extended but finite period of time.

#### 4.4. Accretion onto the secondary

Most of the mass lost by the primary eventually becomes bound to the secondary. One way to look at the accretion is to look at the origin of the particles making up each component. This is shown in Figure 10, where we plot the origin of the particles in the orbital plane and where red and blue dots are particles that were initially bound to the primary and secondary respectively. This colour-coded representation allows us to track the particles as they are shuffled around and become bound to any of the components of the system (i.e. the secondary, the binary envelope, or the ejecta). In the case of the low-mass binary, we see that the secondary is not strongly affected by the infalling material as none of its own particles are being mixed up with the material from the primary. As a matter of fact, the secondary is so

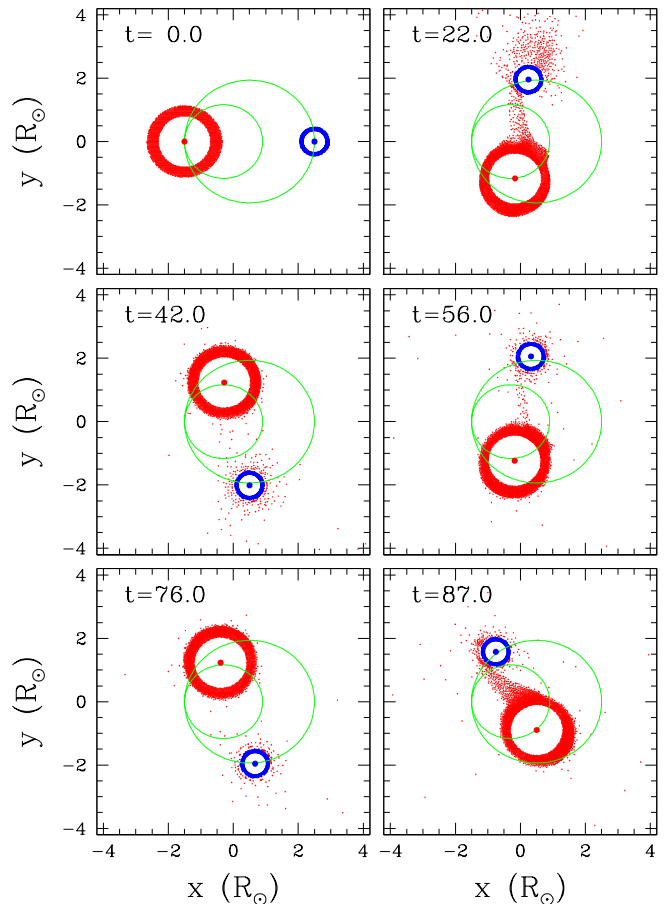


FIG. 10.— Origin of particles in the orbital plane for the  $0.80+0.48 M_{\odot}$  binary with  $e = 0.25$ . Red and blue dots are particles that initially come from the primary and secondary respectively. The time is shown in units of the dynamical timescale ( $\tau_{dyn}$ ) and the orbital period is  $\sim 32 \tau_{dyn}$ . In this case, the secondary is not affected by the infalling material.

dense that it is not perturbed at all by the mass transfer episodes and its accreted material simply forms an envelope around it. Despite this large density gradient at the surface, we note that the interaction between the infalling material from the primary and the secondary's envelope is relatively smooth and no shocks are observed at the surface of the boundary. The smoothing lengths of the transferred particles are consistently adjusted in time (see §3) and are of the same order of magnitude as those of the particles at the surface of the secondary. Also, the difference in mass between the particles being transferred and the particles forming the outer layers of the secondary differs by less than one order of magnitude and we do not observe spurious motions in the envelope suggesting interactions between particles with extreme mass ratios (see e.g. Lombardi et al. 1999). The density contrast can also be observed in Figure 11, which shows a SPLASH three-dimensional surface rendition of the  $0.80 + 0.48 M_{\odot}$  system with  $e = 0.25$ . The surfaces are rendered by defining a critical surface through which we can not see, similar to an optical depth. This three-dimensional rendition allows for the visualization of the whole system. We see that the material transferred from the primary initially forms a thick torus-like cloud around the secondary, and subsequent episodes of



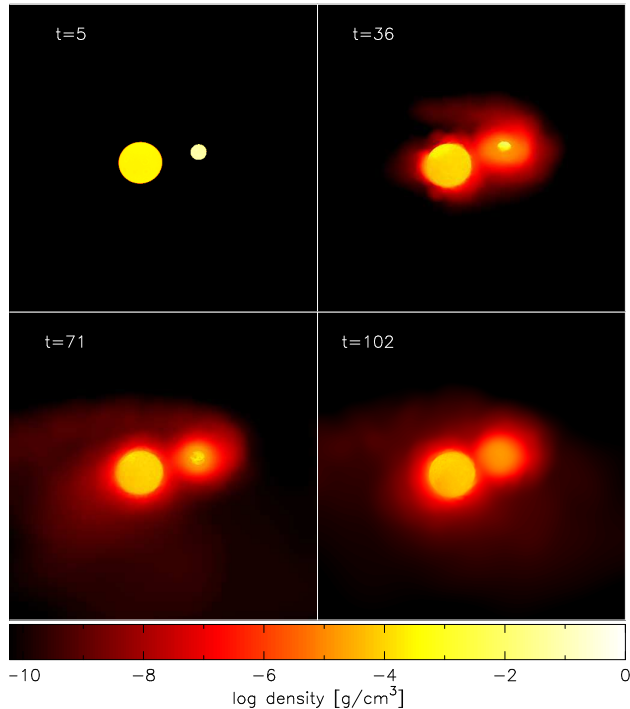


FIG. 11.— Surface rendition (with  $\tau = 0.08$ ) of the density for the  $0.80+0.48 M_{\odot}$  binary with  $e = 0.25$  showing the accretion around the secondary. The time is shown in units of the dynamical timescale ( $\tau_{dyn}$ ) and the orbital period is  $\sim 32 \tau_{dyn}$ . Initially, a thick disk forms around the secondary, but later engulfs it almost completely. Mass loss occurs also primarily from the secondary’s far side, at the  $L_2$  point.

mass transfer eventually form an envelope that rather engulfs the secondary and corotates with it. Moreover, the primary also becomes engulfed by a thin envelope. Since the secondary does not lose any mass, this envelope, as well as the binary ejecta, is made up of the material from the primary.

In the case of the high-mass binary, the similar densities of the two stars allows for the material being transferred to interact much more strongly with the secondary’s envelope, as shown in Figure 12 (for  $e = 0.30$ ). As shown by the red and blue dots, particles from the outermost layers of the secondary, as well as from the primary, are lost from both stars and scattered everywhere in the orbital plane. Although the secondary loses almost as many particles than the primary, the total mass lost by the secondary actually remains relatively small ( $\sim 5\%$  for the  $e = 0.30$  and  $\sim 10\%$  for the  $e = 0.25$  case, at the end of both simulations). Again, we emphasize that the fact that the secondary loses some mass is the result of both the secondary slightly overflowing its Roche lobe (see upper right panel of Figure 12 for example) and the interaction of the infalling material plowing through the envelope of the secondary. This is more analogous to a so-called “direct impact” where the secondary fills most of its Roche lobe and therefore is hit almost right after the transferred material passes the  $L_1$  point. Interestingly, we do not observe such a mass loss from the secondary for smaller eccentricities (e.g.  $e = 0.15$  and  $e = 0.20$ ), which agrees with the fact that only at (relatively) high eccentricity does the system come close to contact. As can be also seen in Figure 13, all of the ma-

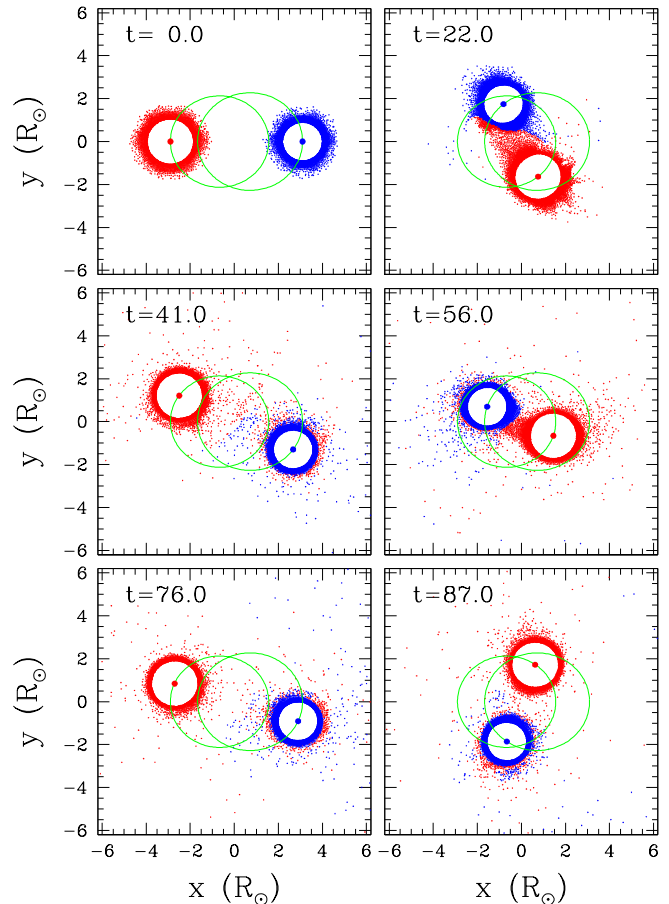


FIG. 12.— Origin of particles in the orbital plane for the  $1.50+1.40 M_{\odot}$  binary with  $e = 0.30$ . Red and blue dots are particles that initially come from the primary and secondary respectively. The time is shown in units of the dynamical timescale ( $\tau_{dyn}$ ) and the orbital period is  $\sim 39 \tau_{dyn}$ . In this case, the secondary loses material because of partial Roche lobe overflow and the interaction of the infalling material with its envelope.

terial being lost from both stars eventually engulfs the whole system rather than forming an envelope around the secondary only. This envelope is substantially denser and thicker than in the low-mass binary case (see Figure 11) as the surface rendition of Figure 13 uses a much larger optical depth in order to peer through the envelope and see the surface of the stars. We observe the formation of such an envelope in all of our simulations for this binary, although the envelope for the  $e = 0.15 - 0.20$  cases is thinner as less material is lost from either star. We note that in the high-mass binaries, the particle mass profiles in both stars are almost identical and we expect and, in fact, observe no spurious motion in the envelope. Similarly, the smoothing lengths are consistently evolved such that particles in regions of similar density have similar smoothing length, allowing for a better spatial resolution.

As in the case of the mass transfer episodes, the accretion episodes also display similar positions and duration and characteristic shapes of Gaussian functions. Our results are again displayed in Table 2. The position of the peaks and the width of the Gaussian are similar to the mass transfer episodes of the primary. The Gaussian parameters for the accretion onto the secondary follow the same trends as shown in Figure 9, with only minor differ-

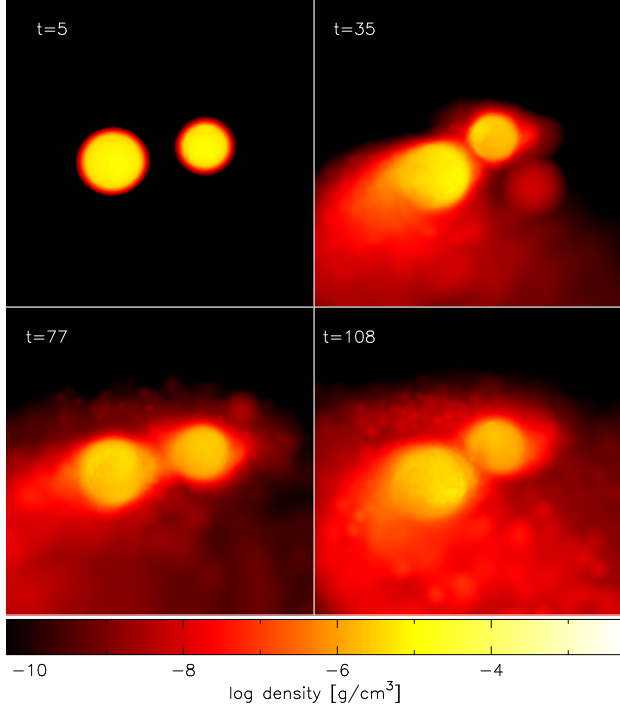


FIG. 13.— Surface rendition (with  $\tau = 25.0$ ) of the density for the  $1.50+1.40 M_{\odot}$  binary with  $e = 0.30$  showing the accretion around the secondary. The time is shown in units of the dynamical timescale ( $\tau_{dyn}$ ) and the orbital period is  $\sim 39 \tau_{dyn}$ . In this case, an envelope engulfs both star and mass loss occurs also from the far side of both stars, at the  $L_2$  and  $L_3$  points

ence in the width of the Gaussians ( $\sigma$ ). Indeed, we notice only a slightly larger spread in  $\sigma$  for the accretion rate when compared with the mass transfer rates. Although we could expect the maximum mass transfer rate ( $A_1$ ) to be larger than the maximum accretion rate ( $A_2$ ), we see that it is not always the case. The reason is simply that the values of the continuum (parameter  $D$ ) are different for the primary and the secondary, thus yielding a different zero level from which the peak values are measured. In any case however, the total mass accreted by the secondary is always less (or equal) to the mass lost by the primary. The remaining mass is obviously lost to the binary as a whole or to the ejecta, which is what we discuss next.

#### 4.5. Mass loss

We now quantify the amount of mass lost to either the binary envelope or the ejecta in our simulations. Particles are assigned to either of these two components if they are far enough from either stellar components and/or their total (relative) energy is positive (see Paper I).

##### 4.5.1. Escaping Particles

Escaping particles are particles that are found far (i.e. many smoothing lengths) from the bulk of the particles. By design, the code, and more specifically the tree building and the neighbours search, run into some problems when particles escape and/or are found in between the two stars, with only a few other close particles. Indeed, when particles are ejected from the system, the search for the required number of neighbours become lengthy and sometimes unsuccessful. To circumvent this issue,

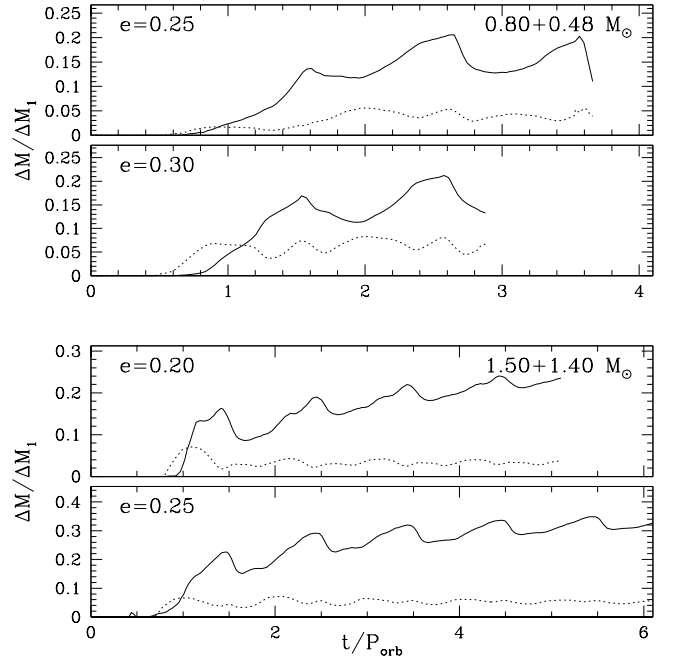


FIG. 14.— Changes in mass in the binary envelope and ejecta normalized by the change in mass of the primary for selected runs for both the  $0.80+0.48 M_{\odot}$  (upper two panels) and the  $1.50+1.40 M_{\odot}$  (lower four panels) binaries. In all cases,  $\sim 5\%$  of the mass lost by the primary ends up in the ejecta.

we set a maximum smoothing length ( $\sim 5 R_{\odot}$ ) such that the code does not unnecessarily spend CPU time iterating and adjusting the smoothing length of a small set of escaping particles (see also §3). These escaping particles lack sufficient neighbours, but their low numbers and total mass are small and do not affect the (hydro)dynamics of the mass transfer process itself.

##### 4.5.2. Binary envelope and ejecta

We now assess the degree of mass loss during the mass transfer episodes in our simulations. We find that in all cases, the mass contained in the binary envelope is greater than that in the ejecta, by a factor of at least two. Both the binary envelope and the ejecta grow in mass as a function of time, and although no clear episodes of mass growth is observed for the ejecta, we observe a stepwise increase in the mass bound to the binary envelope. The total mass in each component ranges from a few  $10^{-7} M_{\odot}$  for the high-mass binary to  $\sim 6 \times 10^{-5} M_{\odot}$  for the low-mass binary. This amounts to  $\sim 0.1-1\%$  of the total initial mass (in SPH particles) of the primary.

Figure 14 shows the change in bound mass of the binary envelope and the ejecta normalized by the change in mass of the primary. Essentially, this shows the fraction of the mass lost by the primary that ends up in the binary envelope or the ejecta. Interestingly, the fraction of mass bound to the binary envelope shows some periodic behaviour, peaking shortly *before* periastron, where the stars are at their closest separation along the orbit. This lag comes from the fact that (some of) the infalling material only temporarily becomes bound to the secondary before becoming bound to the envelope or the ejecta. By the end of our simulations, around 20% of the mass lost by the primary end up in the binary envelope, and our results suggest that this fraction slowly increases as a

function of time.

The mass in the ejecta, on the other hand, is roughly constant around 5% for all of our simulations. This is an unexpected result, given that we observe this trend in all of our simulations, no matter the mass of the stars or the eccentricity. Moreover, given that the degree of mass loss in binary evolution is rather unconstrained (e.g. SWKR09), this result is suggestive of an almost uniform mass loss over different binary masses. Although conservative mass transfer is usually employed as an idealized case, the constant and small fraction of mass lost in our simulations suggests that mass transfer is indeed non-conservative but only to a small degree. This is also interesting in the context of two (slightly) different accretion scenarios, where accretion occurs via an accretion disk or through a direct impact. In the latter case, when the secondary fills a significant fraction of its Roche lobe, the matter falling in from the  $L_1$  point hits the accretor almost directly, whereas in the former case, material falls deep in the potential well of the secondary and forms a disk. Although the direct impact scenario is more representative of our high-mass binary rather than the low-mass binary, and whether or not the infalling material interacts with the secondary's envelope, we still get that roughly 5% of the mass lost by the primary ends up in the ejecta. Note, however, that our simulations do not allow us to assess the fate of the binary envelope. i.e. whether it is going to be expelled from the system and become part of the ejecta or be accreted by either star.

## 5. COMPARISONS WITH PREVIOUS WORK

Similarly to Church et al. (2009), our results show that the mass transfer rates get increasingly larger as the stars get closer to each other at periastron. Moreover, our results indicate that the mass transfer episodes do not occur precisely at periastron and last for a constant fraction of the orbital period, independent of the eccentricity. However, unlike Church et al. (2009), our mass resolution does not allow us to resolve mass transfer rates as low as  $\sim 10^{-10} - 10^{-9} M_\odot \text{ yr}^{-1}$ . Having a better mass resolution would help increase the number of particles in the stream of material for our low-eccentricity binaries, but we do not expect that this would drastically change our conclusions.

Our binaries are set up such that they are in corotation at apastron, therefore making them subsynchronous at periastron. In both of our sets of simulations, the ratio of the angular velocity, which is fixed for the whole duration of the simulations, to the orbital velocity at periastron ranges from around 0.30 to 0.60. Thus, according to Sepinsky et al. (2007a), this has the effect of slightly increasing the Roche lobe radius, by  $\sim 5\%$ , when compared to the instantaneous Roche lobe radius at periastron. Such an increase would therefore effectively *decrease* the degree of overflow and, consequently, the mass transfer rate.

Comparing the magnitude of the mass transfer rate observed in our simulations with theoretical expectations is difficult because estimates of the actual radius of the primary from our simulations are uncertain. Nevertheless, we build a simple model for mass transfer using the (dynamical) mass transfer rate derived for polytropes of index  $n$  by Paczyński & Sienkiewicz (1972) (see also Edwards & Pringle 1987; Eggleton 2006; Gokhale et al.

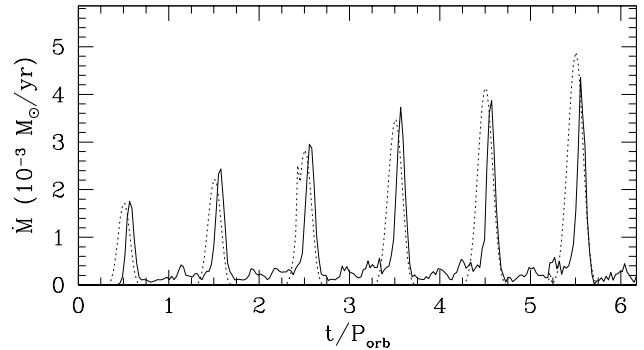


FIG. 15.— Comparison between the instantaneous mass transfer rate of Equation 2 (dotted) and our results (solid) for the the  $1.50 + 1.40 M_\odot$  binary with  $e = 0.25$ .

2007),

$$\dot{M}_1 = -\dot{M}_0 \left( \frac{R - R_L^{inst}}{R} \right)^{n+3/2}, \quad (2)$$

where  $\dot{M}_0$  is a canonical mass transfer rate.  $R_L^{inst}$  is the instantaneous Roche lobe radius, i.e. a simple generalization of the Roche lobe radius for circular and synchronous binaries (Eggleton 1983):

$$R_L^{inst} = D(t) \frac{0.49q_1^{2/3}}{0.6q_1^{2/3} + \ln(1 + q_1^{1/3})}, \quad (3)$$

where  $D(t)$  is the instantaneous separation of the two stars. This mass transfer rate, which applies when the donor can be approximated by a polytrope, depends strongly on the degree of overflow, as expected, and is equally zero when  $\Delta R \leq 0$  (this rate is somewhat different than that of Ritter (1988), which applies when the photosphere is resolved). Starting with the primary's radius as measured at the start of our simulation, i.e.  $R_1 \simeq 1.8R_\odot$ , we calculate the instantaneous degree of overflow,  $\Delta R$ , based on the instantaneous separation of the stars, and a mass transfer rate. This is shown in Figure 15 for the high-mass binary with  $e = 0.25$ . We have arbitrarily set the canonical mass transfer rate ( $\dot{M}_0 \simeq 10^{-1} M_\odot \text{ yr}^{-1}$ ) such that the first peak of mass transfer matches that from our simulation. Moreover, to mimic the slightly increasing peak mass transfer rate, as can be observed in our simulations, we assume that the radius of the star increases at apastron passage by increments of  $0.05 R_\odot$ . We do not expect the radius of the primary to change by much over the course of our simulations since the total mass transferred is small, and this artificial (and rather large) change in radius simply allows for a better match with the increasing peak mass transfer rates. We also note that we see no reasons why both the canonical mass transfer rate  $\dot{M}_0$  and the polytropic index  $n$  should remain constant as mass transfer proceeds, although we have assumed so here, which could compensate for changes in radius. The difficulty in doing such a comparison *with eccentric orbits* lies in the facts that we are using the instantaneous Roche lobe radius derived for circular and synchronous binaries and that the theoretical mass transfer rate used here was derived for polytropes of constant  $n$ . Although this simple model agrees qualitatively well with our simulations (e.g. Gaussian-like episodes of mass transfer), we emphasize

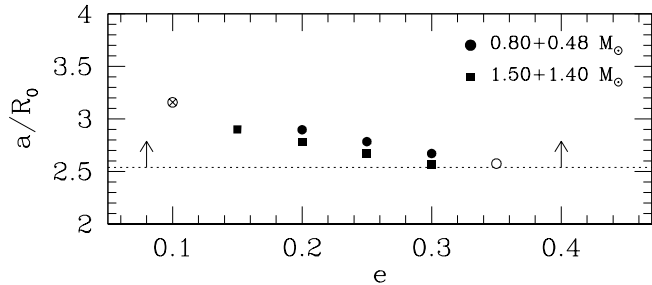


FIG. 16.— Semi-major axis normalized by the initial radius of the primary as a function of eccentricity for all of our simulations. Solid dots are our successful runs, open dots are runs for which mass transfer was too large for our boundary conditions to handle, and open-crossed symbols are for cases when mass transfer was too low or not resolved. The dotted line represents an approximate delimitation above which our boundary conditions can be applied.

that we arbitrarily fixed the canonical mass transfer rate so that the peaks match. However, we observe that the position and width of the mass transfer episode strikingly differ from the theoretical expectation. The width of the peaks depends on the star’s radius, as a shrinking star would delay the start of mass transfer (as well as decrease the degree of overflow), therefore decreasing the mass transfer rate. On the other hand, there is no parameter that could account for the position of the maximum rates as, by construction, the largest degree of overflow occurs when the stars are closest to each other, i.e. at periastron.

## 6. CONCLUSIONS AND FUTURE WORK

The evolution of binary stars has grown into an intense field of study since it has become clear that many populations of stars have to form through interactions with close stellar companions. Although the main phases of binary evolution are nowadays well understood, these evolutionary paths usually rely on the (idealized) formalism derived for *circular* and *synchronized* orbits. This so-called Roche lobe formalism does not apply for close and interacting *eccentric* binaries, in which the rotation is asynchronous and the gravitational potential time-dependent. Given the relatively large number of binary stars, and in particular, of binary stars with eccentric orbits, it is imperative to better understand the interactions of these systems in order to further constrain the different galactic populations of exotic stars. Recent breakthroughs by Sepinsky et al. (2007a), SWKR07 and SWKR09, in particular, have allowed to extend the knowledge of the long-term evolution of eccentric binaries. Although these works clearly show that eccentric binaries behave differently from circular ones, their conclusions are based on a number of assumptions. In this paper, we have presented the results of SPH simulations with the aim of constraining these assumptions.

The results from our large-scale simulations are interesting both for the performances of our alternate approach (see Paper I) and for the characterization of

the mass transfer episodes. Our boundary conditions can effectively handle intermediate mass transfer rates ( $\sim 10^{-6} - 10^{-4} M_{\odot} \text{ yr}^{-1}$ ), although particles penetrate the boundary when the periastron distance is such that the mass transfer rates become too large. On the other hand, our code, by design, does not handle cases where only a handful of particles are transferred. The parameter space where our technique can be applied is therefore restricted by these two conditions on the number of particles. Figure 16 summarizes the orbital parameters for which our technique is well suited. We see that when the normalized semi-major axis is greater than  $\sim 2.5 R_{\odot}$ , our boundary conditions behave well as the mass transfer rates are not excessively large. Also, the use of more lower-mass particles would help resolve lower mass transfer rates and allow for the modeling of systems with higher  $a/R_{\odot}$  values.

The results from our simulations of mass transfer also show clear trends. In particular, we show that the episodes of mass transfer can be described by Gaussians with a FWHM of  $\sim 0.12 - 0.15 P_{\text{orb}}$ , and the peak mass transfer rates occur after periastron, around an orbital phase of  $\sim 0.55 - 0.56$ . It is interesting to note that these results apply for both of the binary systems modeled and for any eccentricity. The technique used in this work represents an interesting alternative to previous work (e.g. Edwards & Pringle 1987, Regös et al. 2005, Church et al. 2009) and we suggest that our results on the properties of interacting eccentric main-sequence binaries could be used in analytical work such as that of SWKR07 and SWKR09 to further constrain the evolution of such stars. We also discussed the accretion onto the secondary and showed that it is also well characterized by similar Gaussians. The accreted material is observed to form a rather sparse envelope around the secondary, in the low-mass binary, and around both stars, in the high-mass binary. Although the fate of this envelope is not determined using our method (whether it is going to be accreted onto either stars or ejected from the system), we showed that a constant fraction of the material lost by the primary is ejected from the systems. Although poorly constrained, the concept of non-conservative mass transfer is generally accepted nowadays and our results may help constrain the degree of mass conservation in binary evolution. In the future, we hope to cover more of the parameter space ( $q$ ,  $a$ , and  $e$ ) in order to get a better picture of mass transfer in eccentric binaries.

We wish to thank the anonymous referee as well as Doug Welch and James Wadsley for useful discussions about this project. This work was supported by the Natural Sciences and Engineering Research Council of Canada (NSERC) and the Ontario Graduate Scholarship (OGS) programs, and made possible in part by the facilities of the Shared Hierarchical Academic Research Computing Network (SHARCNET: [www.sharcnet.ca](http://www.sharcnet.ca)).

## REFERENCES

- Bate, M.R., Bonnell, I.A., & Price, N.M. 1995, MNRAS, 277, 362  
 Benz, W. 1990, in Buchler J.R., ed. The Numerical Modeling of Nonlinear Stellar Pulsations: Problems and Prospects. Kluwer, Dordrecht, p.26 9  
 Church, R.P., Dischler, J., Davies, M.B., Tout, C.A., Adams, T., & Beer, M.E. 2009, MNRAS, 395, 1127  
 D’Souza, M.C.R., Motl, P.M., Tohline, J.E., & Frank, J. 2006, ApJ, 643, 381

- Dermine, T., Jorissen, A., Siess, L., & Frankowski, A. 2009, *A&A*, 507, 891
- Deupree, R.G., & Karakas, A.I. 2005, *ApJ*, 633, 418
- Edwards, D.A., & Pringle, J.E. 1987, *MNRAS*, 229, 383
- Eggleton, P.P. 1983, *ApJ*, 268, 368
- Eggleton, P.P. 2006, *Evolutionary Processes in Binary and Multiple Stars*. Cambridge Univ. Press, Cambridge
- Gokhale, V., Peng, X.M., & Frank, J. 2007, *ApJ*, 655, 1010
- Guenther, D.B., Demarque, P., Kim, Y.-C., & Pinsonneault, M.H. 1992, *ApJ*, 387, 372
- Han, Z., Tout, C.A., & Eggleton, P.P. 2000, *MNRAS*, 319, 215
- Hurley, J.R., Tout, C.A., & Pols, O.R. 2002, *MNRAS*, 329, 897
- Iben, I. Jr 1991, *ApJS*, 76, 55
- Iben, I. Jr, & Livio, M. 1993, *PASP*, 105, 1373
- Ivanova, N., Belczynski, K., Fregeau, J.M., & Rasio, F.A. 2005, *MNRAS*, 358, 572
- Lajoie, C.-P., & A. Sills, 2010, *ApJ*, submitted
- Layton, J.T., Blondin, J.M., Owen, M.P., & Stevens, I.R. 1998, *New Astron.*, 3, 111
- Lombardi, J.C. Jr., Sills, A., Rasio, F.A., & Shapiro, S.L. 1999, *J. Comput. Phys.*, 152, 687
- Lombardi, J.C. Jr., Proulx, X.F., Dooley, K.L., Theriault, E.M., Ivanova, N., & Rasio, F.A. 2006, *ApJ*, 640, 441
- Monaghan, J.J. 1989, *J. Comput. Phys.*, 82, 1
- Morton, D.C. 1960, *ApJ*, 132, 146
- Paczynski, B. 1965, *Acta Astron.*, 15(2), 89
- Paczynski, B. 1971, *ARA&A*, 9, 183
- Paczynski, B., & Sienkiewicz, R. 1972, *Acta Astron.*, 22, 73
- Petrova, A.V., & Orlov, V.V. 1999, *AJ*, 117, 587
- Portegies Zwart, S.F., & Verbunt, F. 1996, *A&A*, 309, 179
- Press, W.H., Teukolsky, S.A., Vetterling, W.T., & Flannery, B.P. 1992, *Numerical Recipes in Fortran*, Cambridge Univ. Press, Cambridge
- Price, D.J. 2007, *Publ. Astron. Soc. Aust.*, 24, 159
- Raguzova, N.V. & Popov, S.B. 2005, *Astron. Astrophys. Trans.*, 24, 151
- Regös E., Bailey, V.C., & Mardling, R. 2005, *MNRAS*, 358, 544
- Ritter, H. 1988, *A&A*, 202, 93
- Rosswog, S., Speith, R., & Wynn, G.A. 2004, *MNRAS*, 351, 1121
- Sepinsky, J.F., Willems, B., & Kalogera, V. 2007a, *ApJ*, 660, 1624
- Sepinsky, J.F., Willems, B., Kalogera, V., & Rasio, F.A. 2007b, *ApJ*, 667, 1170 (SWKR07)
- Sepinsky, J.F., Willems, B., Kalogera, V., & Rasio, F.A. 2009, *ApJ*, 702, 1387 (SWKR09)
- Sills, A.I., & Lombardi, J.C.Jr 1997, *ApJ*, 484, L51

TABLE 1  
PARAMETER SPACE EXPLORED OF BOTH BINARIES MODELED IN THIS WORK.

System	$r_{ap}$ ( $R_{\odot}$ )	$e$	$a$ ( $R_{\odot}$ )	$r_{peri}$ ( $R_{\odot}$ )	# orbits	Mass transfer	Notes
0.80 + 0.48 $M_{\odot}$	4	0.10	3.63	3.27	1.0	N	—
	4	0.20	3.33	2.66	1.0	Y	1
	4	0.25	3.20	2.40	3.5	Y	—
	4	0.30	3.07	2.15	3.0	Y	—
	4	0.35	2.96	1.92	0.5	Y	2
1.50 + 1.40 $M_{\odot}$	6	0.15	5.22	4.43	4.0	Y	—
	6	0.20	5.00	4.00	5.0	Y	—
	6	0.25	4.80	3.60	6.0	Y	—
	6	0.30	4.62	3.23	3.0	Y	3

NOTE. — 1: only a few particles transferred. 2: mass transfer rate too large for the boundary to handle at first periastron passage; particles penetration. 3: mass transfer rate becomes too large after three orbits. See text for more details.

TABLE 2  
GAUSSIAN PARAMETERS FOR THE MASS TRANSFER AND ACCRETION EPISODES OF BOTH BINARIES MODELED IN THIS WORK.

System	$e$	$A_1$ ( $M_{\odot}/\text{yr}$ )	$A_2$ ( $M_{\odot}/\text{yr}$ )	$\mu_1$ ( $P_{\text{orb}}$ )	$\mu_2$ ( $P_{\text{orb}}$ )	$\sigma_1$ ( $P_{\text{orb}}$ )	$\sigma_2$ ( $P_{\text{orb}}$ )	
0.80 + 0.48 $M_{\odot}$	0.25	$9.61 \times 10^{-2}$	$9.60 \times 10^{-2}$	0.60	0.60	0.049	0.048	
		$2.23 \times 10^{-2}$	$2.23 \times 10^{-2}$	1.67	1.67	0.053	0.049	
		$7.06 \times 10^{-2}$	$7.17 \times 10^{-2}$	2.73	2.73	0.049	0.049	
		$3.42 \times 10^{-1}$	$3.45 \times 10^{-1}$	3.65	3.65	0.032	0.030	
	0.30	$5.53 \times 10^{-1}$	$5.50 \times 10^{-1}$	0.59	0.58	0.056	0.054	
		$3.27 \times 10^{-1}$	$3.24 \times 10^{-1}$	1.64	1.64	0.056	0.054	
		$5.48 \times 10^{-1}$	$5.57 \times 10^{-1}$	2.69	2.69	0.057	0.055	
1.50 + 1.40 $M_{\odot}$	0.15	$7.97 \times 10^{-6}$	$7.97 \times 10^{-6}$	0.59	0.59	0.051	0.051	
		$1.00 \times 10^{-5}$	$1.00 \times 10^{-5}$	1.58	1.58	0.048	0.048	
		$1.29 \times 10^{-5}$	$1.29 \times 10^{-5}$	2.58	2.58	0.058	0.058	
		$1.22 \times 10^{-5}$	$1.22 \times 10^{-5}$	3.57	3.57	0.065	0.065	
	0.20	$1.16 \times 10^{-4}$	$1.16 \times 10^{-4}$	0.57	0.57	0.049	0.049	
		$1.22 \times 10^{-4}$	$1.29 \times 10^{-4}$	1.55	1.55	0.066	0.071	
		$1.26 \times 10^{-4}$	$1.33 \times 10^{-4}$	2.55	2.56	0.062	0.063	
		$1.44 \times 10^{-4}$	$1.52 \times 10^{-4}$	3.56	3.56	0.062	0.064	
		$1.38 \times 10^{-4}$	$1.48 \times 10^{-4}$	4.56	4.56	0.065	0.067	
	0.25	$1.80 \times 10^{-3}$	$1.80 \times 10^{-3}$	0.57	0.57	0.041	0.041	
		$2.27 \times 10^{-3}$	$2.29 \times 10^{-3}$	1.57	1.57	0.043	0.043	
		$2.79 \times 10^{-3}$	$2.85 \times 10^{-3}$	2.57	2.57	0.045	0.047	
		$3.35 \times 10^{-3}$	$3.46 \times 10^{-3}$	3.57	3.57	0.045	0.047	
		$3.64 \times 10^{-3}$	$3.79 \times 10^{-3}$	4.56	4.57	0.042	0.045	
		$3.87 \times 10^{-3}$	$4.07 \times 10^{-3}$	5.56	5.57	0.043	0.046	
	0.30	$3.10 \times 10^{-2}$	$3.08 \times 10^{-2}$	0.57	0.57	0.036	0.036	
		$3.41 \times 10^{-2}$	$3.47 \times 10^{-2}$	1.57	1.57	0.037	0.037	
		$4.05 \times 10^{-2}$	$4.13 \times 10^{-2}$	2.57	2.57	0.037	0.037	